The method for the determination of creep cavitation model based on cavity histogram

Xuming Zheng[1], Xin Yang[1], Zhongyu Lu[2] and Qiang Xu[1]
[1]Department of Engineering and Technology, School of Computing and Engineering, University of Huddersfield, UK
[2]Department of Informatics, School of Computing and Engineering, University of Huddersfield, UK
xuming.zheng@hud.ac.uk;
j.lu@hud.ac.uk; ORCID: https://orcid.org/0000-0002-0585-2806;
q.xu2@hud.ac.uk: ORCID: https://orcid.org/0000-0002-5903-9781;

Abstract

Most creep rupture is caused by the cavitation at the grain boundary. Hence it is vitally important to develop a creep cavitation model as it is the prerequisite for the development of the creep cavitation rupture model. Due to the experimental difficulty, it is rare to conduct interrupted creep tests to measure cavity growth. However, cavity histograms were more regularly produced and reported to quantitatively report and record the cavity distribution. This research group originally developed such a concept and the procedures to calibrate the cavitation model reversely based on the cavity histogram. This paper reports and summarizes the detailed work in developing the procedure for the calibration of the cavitation models based on the cavity histogram.

Keywords: cavity nucleation and growth; cavity histogram; creep damage; creep strength; high Cr steel.

1. Introduction

Creep causes various microstructural changes and property deteriorations over time; hence the term damages are introduced. Cavitation at grain boundary is, arguably, the most important one, for most of the high temperature structural materials, with regards to structural integrity. However, this has not been adequately appreciated by research communities and high temperature industries [1-4]. Furthermore, from the methodology point of view, some of the practices adopted in the creep continuum damage mechanics do suffer a few fundamental criticisms [1-10] such as: 1). the phenomenological approach does not actually model the creep cavity damage, only its effect was considered; 2). hence, the coupling of creep cavitation damage and deformation is not mechanism based; and 3). the inability to meet the deformation consistency condition in the multi-axial version of creep damage constitutive equations generalized by the Hayhurst approach. Some pioneer and tentative work was carried out and can be seen in [9-18], but not limited by these.

The challenges involved with creep damage mechanics and creep damage models have been analyzed in the literature review such as those shown initially in [2, 3] and formally in [4]; they are:

(1) Characterizing and quantifying creep cavitation and developing damage criterion for parent metal and weld, respectively; experimental work (uniaxial and multi-axial interrupted

creep test) to be carried out or gathered under low stress; cavitation to be quantified, ideally using X-ray micro-tomography. A new damage criterion shall be developed.
(2) Quantifying the microstructural evolutions and their effects on the creep deformation.
(3) Developing and applying the novel creep formulation suitable for a wider range of stress and incorporating the damage criterion developed in (1).
(4) Generalizing uniaxial version into a three-dimensional creep damage model.

Bearing the above thoughts in mind and particularly on the sight of the published 3D synchrotron creep cavity data for high Cr steels [19], a PhD research project was set up to utilize such valuable data [20]. Its success has opened the door for other projects which investigated other alloys and expanded to use other 3-dimensional cavitation data such as those produced by small angle neutron deflection. A series of publication on the cavitation models and creep lifetime prediction were produced [20-28].

In pursuing the above research, we became aware of and utilized the generic creep cavitation model and creep rupture based on area fraction along the grain boundary model proposed and summarized by Riedel in [23].

The application of Riedel's cavitation model requires 1) a sound understanding of their theories, particularly the theory embodied in the histogram; and 2) a method to determine the values of the five constants in the cavitation model.

It is generally understood and accepted that the best way to obtain the values of the five constants in the cavitation model is through optimization. However, due to the priority of research, we decide to find a practical way to find the numerical answers without having to resort to optimization techniques, although the research group had experience in such a field [29-30].

This paper reports how we devised such practical ways to calibrate the cavitation model practically and quickly.

2. Cavitation model theories

The cavitation nucleation and cavity growth equations are simple enough. The confusion and difficulty are that the cavitation data are typically represented in a histogram; hence an accurate and correct understanding is needed as a prerequisite for the calibration. To understand the concept of histogram, a mathematical textbook such as [31] can be referred to.

The cavitation model theories are summarized in the following. For further details or explanation, see Renversade et al [32] and [4, 24].

The cavity nucleation and cavity growth models are proposed as follows [23]:

$$J^* = A_2 t^{\gamma} \tag{1.1}$$
$$\dot{r} = A_1 r^{-\beta} t^{-\alpha} \tag{1.2}$$

where J^* is the nucleation rate of the cavity, $\dot{r}$ is the non-stationary growth rate of the cavity radius,

r, is the individual cavity size and, t, is the real time, while A_1, A_2, α, β, and γ are material cavitation constants. It is implicitly assumed that they are not changing during the creep process, but they might be dependent on stress.

Some preliminary explanation of their physical meaning and their significance can be found from literature, such as in [23, 32].

A generic cavity size distribution function at time t was proposed by Riedel [23] and it is shown as:

$$N(R,t) = \frac{A_2}{A_1} R^{\beta} t^{\alpha+\gamma} \left(1 - \frac{1-\alpha}{1+\beta} \frac{R^{\beta+1}}{A_1 t^{1-\alpha}}\right)^{(\alpha+\gamma)/(1-\alpha)} \quad (2)$$

where R is cavity radius, $N(R, t)$ is the number of cavitation.

There are five cavitation constants here, namely, α, β, γ, A_1 and A_2, in total. Beware of the definition of R in the N-R space, as it differs from r.

3. Determination methods [4, 20, 24] and Experimental data

Mathematically, Equation (1) will uniquely decide Equation (2), and vice versa, so they are equivalent. Hence Xu concluded that:

1. We can determine the values for the cavitation model based on the data in histogram only, and there is no need for any other experimental data such as the direct measurement of the cavity growth rate and/or the change of cavity number over time.
2. The standard approach would be resorting to optimization techniques.
3. Without resorting to optimization, a set of values can be obtained by solving five independent equations, simultaneously, without the optimization, and there are standard procedures for this task.
4. Even more practical, the trial and error method can be used to construct a theoretical histogram, and through comparison of the predicted histogram and experimental data, and this can be very easily achieved by programming with Excel.
5. The known typical values for any variable can be used as a good starting point, which will reduce the order of difficulty and complexity.
6. If the characteristic values for α and β have been obtained and the value for γ has been suggested for a specific test, then the inner code of the calibration is reduced to find the solution for A_1 and A_2, given set values of α, β and γ. The predicted r-t and N-t at t_f was used to construct the N (R, t_f).
7. The outside loop can be performed for various values for α, β and γ, the sensitivity of the values of α, β, γ can be explored afterwards.

This report will focus on the above point 6. The sensitivity study following the above point 7 was conducted but was not reported here in order to concentrate on the former.

The experimental histogram data was chosen for P91 (9Cr–1Mo–V–Nb) steel at 575°C and was shown in Figure 1 [32]. The leftmost and rightmost points were used for our calculation and

illustration. They are t_f =10200 h, respectively, R_1= 0.6μm, N (R_1, t_f) =3800 and R_2 = 2.4μm, N (R_2, t_f) =1.

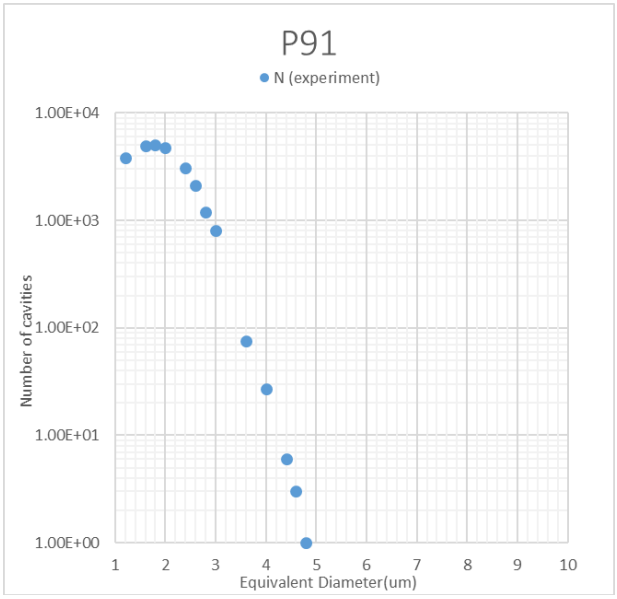

Figure 1. The experimental histogram data for P91 steel [32].

In the cavity size-time space, the maximum cavity r is r_i and r_j corresponding to real time t_i and t_j. Further mathematical equations for calibration are shown as follows:

$$N(R,t_f)=\frac{A_2}{A_1}R^{\beta}{t_f}^{1+\gamma}exp\left(-\frac{1+\gamma}{1+\beta}\frac{R^{\beta+1}}{A_1}\right) \tag{3}$$

$$\frac{1}{3}r^3=A_1lnt+C \tag{4.1}$$

$$\frac{1}{3}r_i^3=A_1lnt_i+C \tag{4.1a}$$

$$\frac{1}{3}r_j^3=A_1lnt_j+C \tag{4.1b}$$

$$A_1=\frac{R_j^3-R_i^3}{3(lnt_j-lnt_i)} \tag{4.1c}$$

$$A_1=\frac{-2{R_1}^3+2{R_2}^3}{3Ln(N(R_1,t_f){R_2}^2/N(R_2,t_f){R_1}^2)} \tag{4.2}$$

Substitute A_1 into Equation (3) and using the point 2 on the histogram (R_2=2.4μm, N (R_2, t_f) =1), gives:

$$A_2=\frac{N(R_2,t_f)A_1}{{R_2}^2{t_f}^2\exp(-2{R_2}^3/3A_1)} \tag{4.3a}$$

Substitute A_1 into Equation (3) and using the point 1 (R_1= 0.6μm, N (R_1, t_f) =3800), gives:

$$A_2=\frac{N(R_1,t_f)A_1}{{R_1}^2{t_f}^2\exp(-2{R_1}^3/3A_1)} \tag{4.3b}$$

3.1 Forward method [20]

The method consists of the following steps and it is implemented via Excel:

1. From a cavity growth point of view, Equation (4.1c) can be used for the determination of A_1.
2. The first point in t-r space, it is guessed t_i for a given r_i, and the second would be $r_j = R_2$ and $t_j = t_f$. We could take $r_i = R_1$, and the t_i is a guessed value, and it should be relatively very small in comparison with t_f.
3. Then substitutive the known A_1 into Equation (4.3b) to obtain A_2.
4. Based on the known A_1 and A_2, the histogram can be drawn using Equation (3).
5. Based on the difference between the predicted histogram curve with the experimental points, a series of initially estimated time t_i can be tried out to produce the best fit.
6. The integration constant C can be found.

In this method, only one point from the histogram is taken for the determination of the constants.

The values found are:
t_0 = 41.367 h, then it is found that of A_1= 8.2358E-1, A_2= 9.95E-5 and C= -2.9938.

It is worth reporting that when it is difficult to judge which is the best value for t_0 when it is around 41 hours, hence there is a small degree of inaccuracy and uncertainty. In this method, only one point, R_2, from the histogram is directly taken for the determination of the constants. The overall quality of fit is judged in the selection of the trial t_i.

3.2 Xuming Zheng's method [24]

This method is called a backward method, directly taken two points from the histogram, and it finds the values of A_1 and A_2 by solving the two simultaneous Equations (3).

The values are $\alpha = 1$, $\beta = 2$, $\gamma = 1$. We chose the leftmost and rightmost points for our calculation and illustration, they are: t_f=10200 h, respectively, R_1=0.6μm, N (R_1, t_f) =3800 and R_2=2.4μm, N (R_2, t_f) =1.

Specifically,
$$A_1 = \frac{-2{R_1}^3 + 2{R_2}^3}{3Ln(N(R_1,t_f){R_2}^2/N(R_2,t_f){R_1}^2)} \quad (4.2)$$

$$A_2 = \frac{N(R_2,t_f)A_1}{{R_2}^2{t_f}^2\exp(-2{R_2}^3/3A_1)} \quad (4.3a)$$

or
$$A_2 = \frac{N(R_1,t_f)A_1}{{R_1}^2{t_f}^2\exp(-2{R_1}^3/3A_1)} \quad (4.3b)$$

The values found are:
A_1= 8.2358E-1, A_2= 9.95E-5. Then it is found that of C= -2.9938 and t_0 = 41.367 h.

4. Results and Discussion

The results of the forward method are shown in Figure 2 and Figure 3, while the results of the

backward method are shown in Figure 4 and Figure 5.

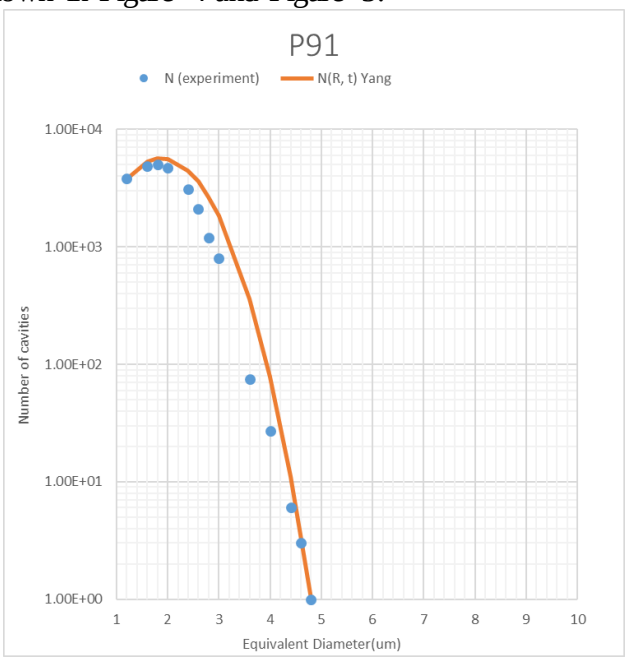

Figure 2. The probability density function of cavity equivalent R for P91 by the forward method [27], compared with the experimental histogram data [32].

Figure 2 is displayed the prediction curve by using Equation (3) with the forward method, which fit well with the experimental data. According to the values of t_0, A_1, C and A_2, the curve can be extended to include the condition of the minimum diameter and it is shown in Figure 3.

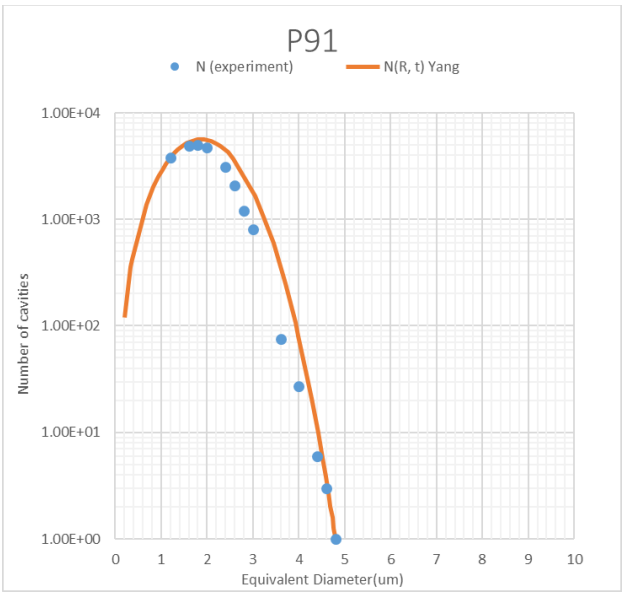

Figure 3. The prediction curve includes the condition of the minimum diameter [27], compared with the experimental histogram data [32].

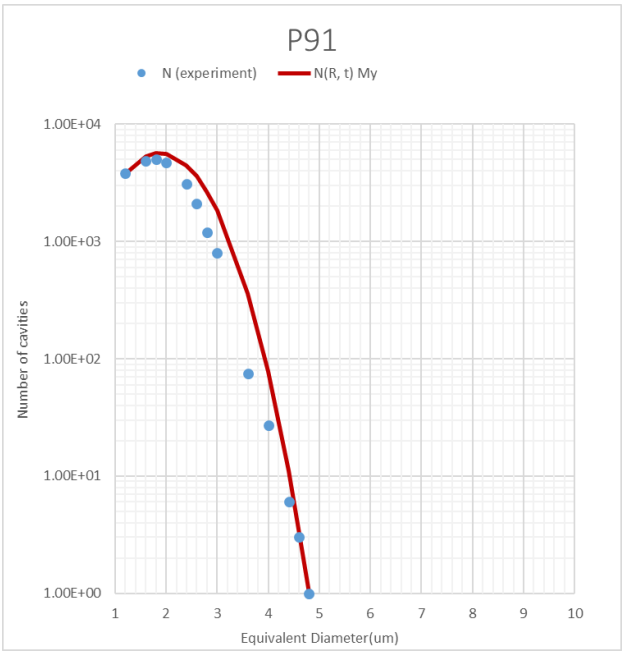

Figure 4. The probability density function of cavity equivalent R for P91 by the backward method [27], compared with the experimental histogram data [32].

Figure 4 is displayed the prediction curve by using Equation (3) with the backward method. The curve fit going through the first and last point because these curves are based on these two points to calculate the values of A_1, A_2 et al. It is not to say that method gives too much weight to those two points. This curve fit better than other curves that are based on another two points for P91 steel. The method is that any two points can be chosen, and the curve can go through these two points necessarily but the curve whether through or nearly the remaining points that is a question. In other words, the trend of the curve is the same as its experimental data and almost points are approaching the curve, this curve based on these two points is the best one. According to the values of t_0, A_1, C and A_2, the curve can be extended to include the condition of the minimum diameter and it is shown in Figure 5.

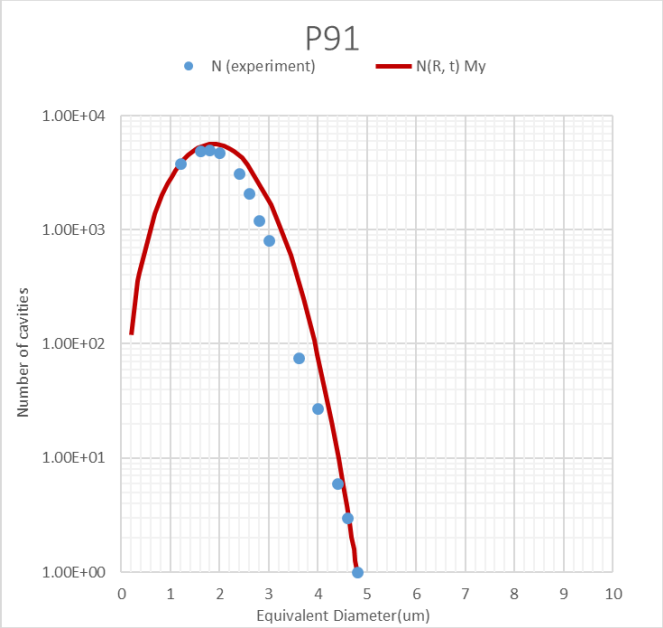

Figure 5. The prediction curve includes the condition of the minimum diameter [27], compared with the experimental histogram data [32].

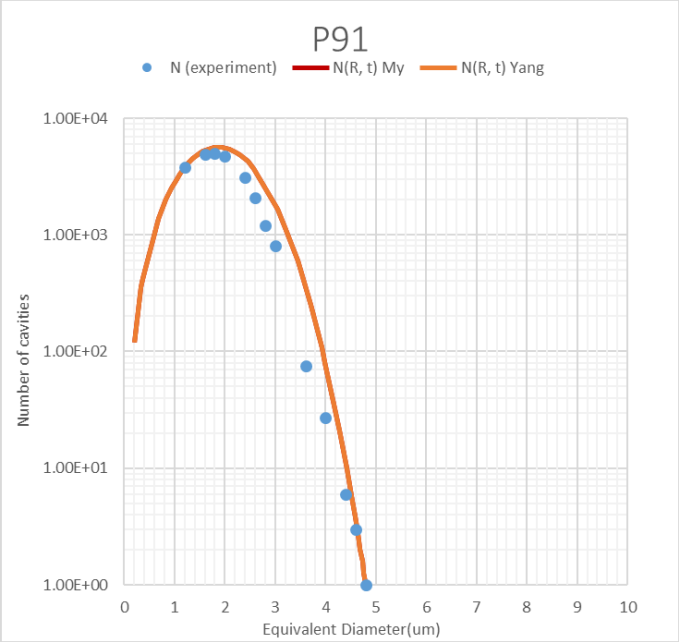

Figure 6. The comparison of the accuracy of the two methods [27], compared with the experimental histogram data [32].

Although in the original forward method, the predicted histogram could be constructed using the predicted r-t and N-t relations at t_f, the Excel file we created for the illustration did use N (R, t_f) equation expressed by Equation (3) directly. The intermediate results with various initial t_i under

a set of α, β and γ are not shown for brevity. The efficiency and convenience of such calculations depend on the parametric coding of the Excel program, the sensitivity study with various α, β and γ were conducted easily, and they are not reported here either.

The comparison of the two methods is shown in Figure 6. It clearly shows that both methods are capable to produce reasonably accurate results and the difference between them is small by the naked eye. The backward method is better than the forward method due to its directness for determining A_1 and A_2. The production of r-t and N-t curves did help to understand the intricate relation of N (R, t_f).

5. Conclusion

As far as the authors are aware of the literature, this is the first time that the method for calibrating a generic cavitation model based on cavity histogram was devised.

The application of the (forward) method enabled the production of the cavitation model, and the derivation of an analytical and explicit creep cavitation damage evolution model. The application of these models will significantly advance the understanding of and modeling of creep damage and rupture.

Parallel to this progress, research on the mesoscopic modeling on the creep deformation and damage has also been undertaken and published [33].

Acknowledgement

Mrs Xuming Zheng and Mr Xin Yang are grateful for the Santander Postgraduate Mobility scheme which enabled them to visit and present their research results to Prof Wang, Wuhan University, China, in 2017.

Reference

1. The development of validation methodology of multi-axial creep damage constitutive equations and its application to 0.5Cr0.5Mo0.25V ferritic steel at 590°C, Xu, Q., 1st Mar 2004, Nuclear Engineering and Design. 228, 1-3, p. 97-106.

2. Damage modelling: the current state and the latest progress on the developing of creep damage constitutive equations for high Cr steels, Xu, Q., Lu, Z. & Wang, X., 2013, 6th International 'HIDA-6' Conference: Life/Defect Assessment & Failures in High Temperature Plant. Shibli, A. (ed.). ETD Ltd, UK.

3. Damage modelling: the current state and the latest progress on the development of creep damage constitutive equations for high Cr steels, Xu, Q., Lu, Z. & Wang, X., 4th May 2017, Materials at High Temperatures. 34, 3, p. 229-237.

4. On the development of creep damage constitutive equations: modified hyperbolic sine law for minimum creep strain rate and stress and creep fracture criterion based on cavity area fraction along grain boundary, Xu, Q., Yang, X. & Lu, Z., 17th Nov 2017, In: Materials at High Temperatures. p. 323-332.

5. Development of constitutive equations for creep damage behaviour under multi-axial states of stress, Xu, Q., 3rd Nov 2000, Advances in Mechanical Behaviour, Plasticity and Damage: Proceedings of EUROMAT 2000, Tours, France, 7-9 November. Berveiller, M. (ed.). 1st ed. Elsevier, Vol. 2. p. 1375-1382.

6. Development of constitutive equations for creep damage behaviour under multi-axial states of stress, Xu, Q., In: Structures and Materials Volume 6, 2000, Pages 435-445 Sixth International Conference on Damage and Fracture Mechanics: Computer Aided Assessment and Control, Damage and Fracture Mechanics 2000; Montreal, Que; Canada; 22nd May 2000 through 24th May 2000; Code 63550.

7. The development of phenomenological multi-axial isotropic creep damage constitutive equations, Xu, Q., 2003, In: Mechanics and Material Engineering for Science and Experiments, Pages 457-460, 2003; Proceedings of the International Symposium of Young Scholars on Mechanics and Material Engineering for Science and Experiments; Changsha/Zhangjiajie; China; 11-16 August 2001; Code 61598.

8. Creep damage constitutive equations for multi-axial states of stress for 0.5Cr0.5Mo0.25V ferritic steel at 590°C, Xu, Q., 1st Oct 2001, Theoretical and Applied Fracture Mechanics. 36, 2, p. 99-107.

9. The evaluation of high-stress creep ductility for 316 stainless steel at 550 °C by extrapolation of constitutive equations derived for lower stress levels, Xu, Q. & Hayhurst, D., 1st Oct 2003, International Journal of Pressure Vessels and Piping. 80, 10, p. 689-694.

10. The development of multi-axial creep damage constitutive equations for 0.5Cr0.5Mo0.25V

ferritic steel at 590ºC, Xu, Q. & Barrans, S., 1st Jan 2003, JSME International Journal Series A. 46, 1, p. 51-59.

11. The development and validation of multi-axial creep damage constitutive equations for P91, Xu, Q., Wright, M., and Xu, Q. 2011 In: Proceedings of 2011 17th International Conference on Automation and Computing, ICAC 2011, 6084923, pp. 177-182.

12. Review on the current state of developing of advanced creep damage constitutive equations for high chromium alloy, An, L., Xu, Q., Xu, D., and Lu, Z. 2012, In: Advanced Materials Research, 510, pp. 776-780.

13. Current state of developing creep damage constitutive equation for 0.5Cr0.5Mo0.25V ferritic steel, Xu, Q., Xu, Q., Pan, Y., and Short, M., 2012, In: Advanced Materials Research, 510, pp. 812-816.

14. Preliminary analysing of experimental data for the development of high Cr alloy creep damage constitutive equations, An, L., Xu, Q., Xu, D., and Lu, Z., 2012, In: ICAC 12 - Proceedings of the 18th International Conference on Automation and Computing: Integration of Design and Engineering, 6330535, pp. 207-211.

15. Review of creep cavitation and rupture of low Cr alloy and its weldment, Xu, Q.H., Xu, Q., Pang, Y.X., Short, M., 2013, In: Advanced Materials Research, 744, pp. 407-411.

16. Analysing the characteristics of the cavity nucleation, growth and coalescence mechanism of 9Cr-1Mo-VNb steel (P91) steel, An, L.L., Xu, Q., Lu, Z.G., and Xu, D.L., 2013, In: Advanced Materials Research, 744, pp. 412-416.

17. The validation of computational FE software for creep damage mechanics, Liu, D.Z., Xu, Q., Lu, Z.Y., Xu, D.L., Tan, F., 2013, In: Advanced Materials Research, 744, pp. 205-210.

18. Preliminary review of the influence of cavitation behavior in creep damage constitutive equations, Yang, X., Xu, Q., Lu, Z.Y., and Barrans, S., 2014, In: Advanced Materials Research, 940, pp. 46-51.

19. Study of creep cavitation behavior in tempered martensitic steel using synchrotron micro-tomography and serial sectioning techniques, Gupta, C., Toda, H. & Schlacher, C., et al., 2013, Mater Sci Eng A. 564:525–538.

20. The development of creep damage constitutive equations for high chromium steel based on the mechanism of cavitation damage, PhD Thesis, Yang, X, 2018, The University of Huddersfield, UK.

21. On the development of creep damage constitutive equations, keynote presentation, Xu, Q., Yang, X. & Lu, Z., 2015 May 15–17, HIDA-7: Life/defect assessment & failures in high temperature industrial structures, Portsmouth: Portsmouth University.

22. The interpretation of experimental observation date for the development of mechanisms based creep damage constitutive equations for high chromium steel, Yang, X., Lu, Z., Xu, Q., 2015, In: 21st International Conference on Automation and Computing: Automation, Computing and Manufacturing for New Economic Growth, ICAC 2015, 7313992.

23. Fracture at high temperatures, Riedel, H., Berlin: Springer Verlag; 1987.10.1007/978-3-642-82961-1.

24. The development of creep damage constitutive equations for high Cr steel, Zheng, X., Xu, Q., Lu, J., Wang, X. & Feng, X., 1st Mar 2020, In: Materials at High Temperatures. 37, 2, p. 129-138.

25. Creep rupture modelling of P92 alloy based on the concept of grain boundary cavitation, Zheng, X.M., Lu, Z.Y., Xu, Q., Dec 2020, Submission to Materials at High Temperatures.

26. Initial calibration of creep cavitation model for 316H steel, Zheng, X.M., Lu, Z.Y., Xu, Q., Dec 2020, Submission to Materials at High Temperatures.

27. The development and application of creep damage constitutive equations for high Cr steels over a wide range of stress, Doctor Thesis, Zheng, X.M., March 2021, The University of Huddersfield, UK.

28. Creep cavitation damage modeling – stress level on 316 alloy, MSc thesis, Fu, G.L., December 2020, The University of Huddersfield, UK.

29. The effect of initial estimated points on objective functions for optimisation, Soltani, M., Pola, A. & Xu, Q., 2014, Proceedings - 28th European Conference on Modelling and Simulation, ECMS 2014. European Council for Modelling and Simulation, p. 304-308.

30. Determination of the material constants of creep damage constitutive equations using Matlab optimisation procedure, Igual, J. Z. & Xu, Q., 30th Oct 2015, 2015 21st International Conference on Automation and Computing: Automation, Computing and Manufacturing for New Economic Growth, ICAC 2015. Institute of Electrical and Electronics Engineers Inc., 7313991.

31. The manager's guide to statistics and quantitative methods, Donald, W., Kroeber and R. Lawrence LaForge., 1980, McGraw-Hill Book Company, ISBN 0-07-035520-7.

32. Microtomographic assessment of damage in P91 and E911 steels after long-term creep, Renversade, L., Ruoff, H., Maile, K., Sket, F., Borbely, A., 2014, International Journal of Materials Research, 105 (7), 621-627.

33. Development of the FE in-house procedure for creep damage simulation at grain boundary level (Open Access), Xu, Q., Tu, J., and Lu, Z., 2019, In: Metals, 9(6),656.